Dynamical properties and instability of local fluorite BaF_2 structure around doped Mn^{2+} ions—EPR and electron spin echo studies

2008 J. Phys.: Condens. Matter 20 385208

(http://iopscience.iop.org/0953-8984/20/38/385208)

J. Phys.: Condens. Matter **20** (2008) 385208 (7pp) doi:10.1088/0953-8984/20/38/385208

Dynamical properties and instability of local fluorite BaF_2 structure around doped Mn^{2+} ions—EPR and electron spin echo studies

S Lijewski[1], S K Hoffmann[1,3], J Goslar[1], M Wencka[1] and V A Ulanov[2]

[1] Institute of Molecular Physics, Polish Academy of Sciences, Smoluchowskiego 17, 60-179 Poznan, Poland
[2] Physical Technical Institute, Russian Academy of Sciences, Sibirski Trakt 10/7, 420029 Kazan, Russia

E-mail: skh@ifmpan.poznan.pl

Received 20 June 2008, in final form 1 August 2008
Published 27 August 2008
Online at stacks.iop.org/JPhysCM/20/385208

Abstract

The electron paramagnetic resonance (EPR) and electron spin echo (ESE) were measured at the X-band for Mn^{2+} in a BaF_2 crystal in the temperature range 4.2–300 K. In addition to the cubic symmetry centre, two other lower concentration tetragonal centres were identified. Temperature variations and computer simulation of the EPR spectrum confirm that the cubic symmetry of the MnF_8 centre is deformed to two T_d tetrahedra of different dimensions at around 45 K. Electron spin relaxation was measured in the temperature range 4.2–35 K, where the ESE signal was detectable. For higher temperature the Mn^{2+} dynamics produces homogeneously broadened EPR lines. At the lowest temperatures the spin–lattice relaxation is governed by ordinary phonon processes with $1/T_1 \sim T^5$. The efficiency of these processes rapidly decreases and at about 11 K a local mode of energy 17 cm^{-1} becomes the relaxation mechanism. Phase relaxation observed as ESE signal dephasing indicates that after the local deformation jumps (tunnelling with frequency 4×10^8 s^{-1}) between the two tetrahedral configurations appear, with the energy barrier being the local mode energy. This motion is directly visible as a resonance-type enhancement of the ESE dephasing rate $1/T_M$ around 11 K. Only the cubic centre displays the above dynamics.

1. Introduction

Fluorite crystals $M^{II}F_2$ (M^{II} = Ca, Ba, Sr, Cd, Pb) have a simple cubic structure in which the divalent cation M^{II} is surrounded by eight fluorine anions located at the corners of the unit cell. Various divalent and trivalent ions of iron group elements and rare-earth elements have been introduced into fluorite lattices to study the local structure of the host lattice and for modification of its dynamics and macroscopic properties. The doped ions influence the optical and luminescent properties of fluorite crystals, which are used as luminophores and as scintillators for γ-ray and elementary particle detection. Fluorite crystals display low dielectric losses and are hard and insoluble in water, allowing effective polishing of crystal surfaces for optical applications. Fluorites are model ionic crystals in solid-state spectroscopy studying phonon spectra and interactions of electromagnetic waves with ionic structures. At high temperatures fluorites become superionic conductors with many potential applications. The cubic fluorite structure is stable under ambient conditions, but under high pressure transitions to two new phases, orthorhombic and hexagonal, appear at 2.84 and 12.8 GPa in BaF_2, with theoretically predicted metallization around 33 GPa [1]. The physical properties of crystals with fluorite structure are described in the book [2] and spectroscopy of

[3] Author to whom any correspondence should be addressed.

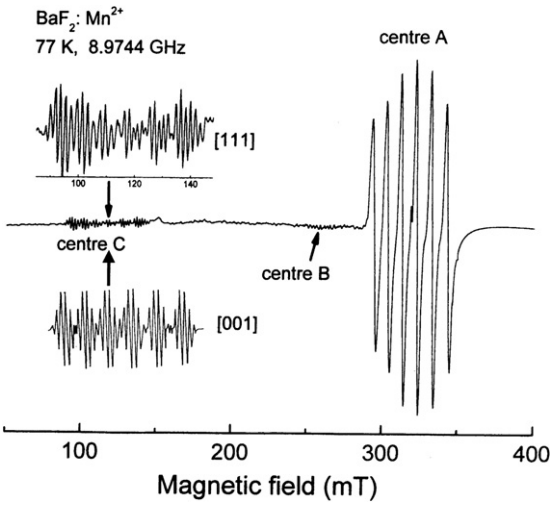

Figure 1. EPR spectrum of Mn^{2+} in a BaF_2 crystal recorded along the [111] direction at 77 K. Centres A, B, and C are marked. Lines of centres C are gained and are additionally shown for the [001] direction at 4.2 K.

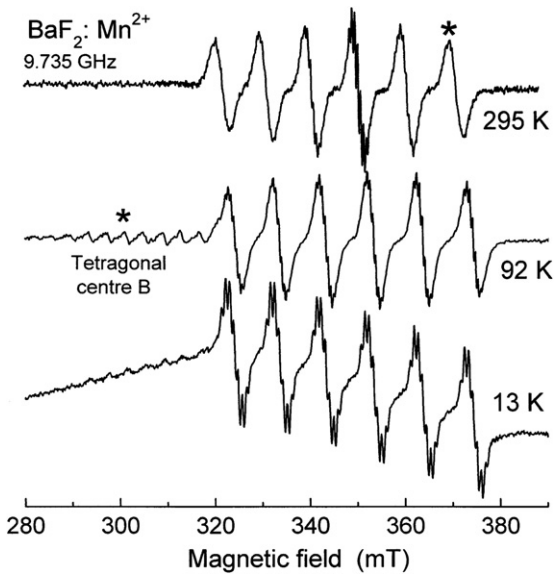

Figure 2. EPR spectra recorded at room temperature, 92 and 13 K along the [110] direction. An asterisk marks the lines excited in electron spin echo experiments.

various doped transitions ions is reviewed in [3]. The transition ions substitute M^{II} host cations and are in a crystal field of cubic O_h symmetry formed by a cube of F^- anions. It allows us to study the ions in cubic eight-coordination, which gives the opposite ground state of the ions as compared to the usual octahedral coordination. Moreover, the fluorine nucleus has relatively large nuclear magnetic moment and $I = 1/2$, thus strong hyperfine metal–ligand coupling allows accurate measurements of interactions of doped ions with host lattice anions.

Mn^{2+} ions are introduced into fluorite crystals for modification of their optical properties and act as luminescence and thermoluminescence centres [4, 5]. Electron paramagnetic resonance (EPR) studies have shown that most of the doped Mn^{2+} ions substitute divalent cations and are surrounded cubically by eight fluorine ions [3, 6–9]. In some cases Mn^{2+} centres with tetragonal and trigonal symmetry have also been found [9–11]. In crystals growing in the presence of residual oxygen or water vapour atmosphere various low symmetry $MnF_{8-x}O_x$ centres was observed [10, 12]. These complexes with impurity oxygen ligands are unstable and disappear after annealing above 800 °C. In x-ray irradiated CaF_2 crystals the Mn^+ centres in a cubic environment have been observed at low temperatures [13, 14].

In the BaF_2 crystal having cubic $Fm3m$ symmetry ($a = 0.6196$ nm, $Z = 4$) the Ba–F distance is 0.268 nm. Due to a small ionic radius of guest Mn^{2+} (0.08 nm), compared to the substituted host Ba^{2+} (0.135 nm), some strains or distortions of the doped BaF_2 lattice can be expected [4]. Moreover, the analogous manganese compound MnF_2 has not cubic but rutile-type tetragonal $P4_2/mnm$ structure containing octahedral MnF_6 complexes with Mn–F distances 0.214 and 0.211 nm. This suggests that the local structure around the doped Mn^{2+} may be unstable or strongly deformed. EPR data indicate that at room temperature Mn^{2+} is located in the centre of the fluorine cube. The EPR [9] and ENDOR [6] data have shown that the structure of the MnF_2 cube in BaF_2 changes when temperature is lowered below about 45 K. It seems that the lattice instability and local dynamics is a general problem in systems with potentially off-centre shift of doped impurities when doped ions of small radius substitute the larger radii host ions. This was clearly recognized in alkali halides doped with Li^+ as reviewed in [15], in fluoride crystals doped with ions Cu^{2+} displaying the dynamic Jahn–Teller effect [16], and in ionic BaO:Mn^{2+} [17] and SrO:Ni^+ [18] crystals.

In this paper we discuss dynamical properties of Mn^{2+} in barium fluoride single crystals observed both in continuous wave EPR spectra and in electron spin echo experiments in the temperature range 4.2–300 K.

2. Experimental details

Deep orange single crystals of BaF_2 doped with Mn^{2+} were grown in a crucible in gaseous helium–fluorine atmosphere by the vertical Bridgman technique as described previously in the synthesis of BaF_2:Cu^{2+} [19]. The concentration of Mn^{2+} ions was evaluated from the EPR spectrum intensity as 4.0×10^{19} ions g^{-1}.

X-band continuous wave EPR and pulsed EPR measurements were performed using a Bruker ESP 380E FT/CW spectrometer with a dielectric TE_{011} resonator. Q-band spectra were recorded using a Varian E-12 spectrometer. Temperature variations of EPR spectra were studied in the temperature range from 4.2 to 300 K using an Oxford CF935 helium flow cryostat. Pulsed EPR measurements were performed within the temperature range from 4 up to 35 K, since above this temperature the electron spin echo signal was too weak to be recorded. The two manganese (II) centres (centres A and B marked in figure 1) were independently excited by microwave pulses at the magnetic field marked by an asterisk in figure 2. The selective pulses excited single hyperfine lines.

The spin–lattice relaxation time was measured using the saturation recovery method. Nearly full saturation was achieved with a 24 ns pulse having 1.76 mT bandwidth. The magnetization recovery was observed by the Hahn-type spin echo using a (24 ns–384 ns–24 ns–echo) pulse sequence. The recovery was exponential for both centres.

The spin echo dephasing (phase relaxation) time T_M was determined from an echo decay experiment with two 24 ns pulses separated by a 384 ns time interval.

3. Results and discussion

3.1. Cw-EPR spectrum and its temperature variations

The EPR spectrum recorded at 77 K along the [111] direction is shown in figure 1. Because of a relatively high Mn^{2+} concentration, three different types of spectrum are visible. In addition to the main cubic spectrum (centre A), two other spectra of lower intensity and lower symmetry (spectrum B and spectrum C) display lines at lower magnetic field. These two spectra have tetragonal symmetry as clearly evidenced for spectrum C when recorded along [001] (see the enlarged part of the spectrum in figure 1). At this crystal orientation spectrum C consists of six hfs lines split into a sextet with intensity ratio 1:5:10:10:5:1 from interaction with five equivalent ^{19}F nuclei ($I = 1/2$). Thus one fluorite ion is missing and probably replaced by an oxygen atom during crystal growth as identified in heavily Mn-doped BaF_2 [12].

The cubic spectrum A is described by the spin Hamiltonian

$$H = g\mu_B \vec{B} \cdot \hat{S} + \tfrac{1}{6}a\left[\hat{S}_x^4 + \hat{S}_y^4 + \hat{S}_z^4 - \tfrac{1}{5}S(S+1) \times \left(3S^2 + 3S - 1\right)\right] + A\hat{S} \cdot \hat{I}^{Mn} + \sum_{i=1}^{8} \hat{S} \cdot T^{F(i)} \cdot \hat{I}^{F(i)} \quad (1)$$

where the first term is the electron Zeeman interaction, with isotropic g-factor equal to 2.0013(0.0005); the second term describes splitting in a cubic field, which is very weak and not resolved in our relatively broad lines. The cubic splitting parameter is about $a = 0.7 \times 10^{-5}$ cm^{-1} [20]. The manganese hyperfine (hf) splitting constant is $A = 91.29(0.1) \times 10^{-4}$ cm^{-1} and the fluorine hf is $T_{\|} = 11.1(0.4) \times 10^{-4}$ cm^{-1} and $T_{\perp} = 5.1(0.4) \times 10^{-4}$ cm^{-1} at room temperature. Fluorine hf structure is badly resolved at [111] orientation but is much better resolved along the [110] direction as visible in figure 2, where the temperature variation of the spectrum is presented. The room temperature spectrum displays a dependence of the individual line on the quantum number m_I, with narrowest lines for $m = +1/2$. This is a well known dynamical effect resulting from the tumbling motion of the manganese ion characteristic for liquids but also reported for VO^{2+} and Mn^{2+} in solids [21–23]. This effect appears when the tumbling frequency is comparable with the linewidth (of the order of tenths of MHz) and gradually vanishes when the temperature is lowered and the tumbling rate decreases. At 77 K this effect is still visible (see also figure 1), but below 20 K hf lines become identical and the lattice can be treated as rigid. Also, the fluorine hf structure changes at low temperatures.

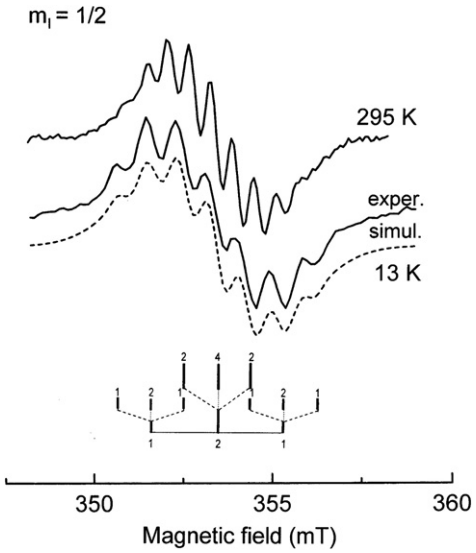

Figure 3. Hyperfine $m_I = +1/2$ line at room temperature and at 13 K showing the change from a nine to a seven line pattern. The low temperature line is simulated (dashed line) with intensity ratio 1:2:3:4:3:2:1 and splitting of $t_F = 0.86$ mT between the lines. The stick diagram below the spectra explains the intensity ratio as due to interaction with four F^-, producing splitting $2t_F$ and t_F.

Down to about 50 K every m_I line consists of nine fluorine lines with amplitude ratio 1:8:28:56:70:56:28:8:1, indicating interaction with eight equivalent fluorine nuclei as expected for the MnF_8 complex. This is illustrated for the $m_I = +1/2$ line in figure 3. Below 50 K a change in the hf structure appears. Instead of nine lines seven lines appear. Computer simulation (dashed line in figure 3) shows the intensity ratio 1:2:3:4:3:2:1, which results from interaction with two pairs of fluorine nuclei, giving a splitting ratio of 2:1 as shown by the stick diagram in figure 3. It should be stressed that the local symmetry around Mn^{2+} is retained and the zero-field splitting is still equal to zero. This was described as a static local lattice distortion around Mn^{2+} with a radial inward shift of the four F^- and a simultaneous outward shift of the other four F^- [4, 8]. Instead of cubic symmetry the new local structure of tetrahedral T_d symmetry is formed, involving two inequivalent F^- tetrahedra and two different Mn–F distances (0.224 and 0.250 nm), as shown in figure 4. This structural change was assumed to be due to a local Mn^{2+} vibration of A_2 symmetry [9] and extensively discussed in terms of density functional theory as due to the anharmonic coupling between a_{2u} and t_{1u} modes [24]. In the low temperature spectrum of figure 3 the magnetic field is directed along the F–F direction of the smaller tetrahedron, thus two of the F^- ions are close to the parallel direction whereas the other two are close to the perpendicular direction. Thus, we observe the splitting from the smaller tetrahedron only. The splitting from F^- of the larger tetrahedron is not resolved. The spin relaxation measurements described in section 3.2 will show that this is due to tunnelling between two equivalent distortions producing line broadening to about 0.46 mT (compared with 0.32 mT at 295 K).

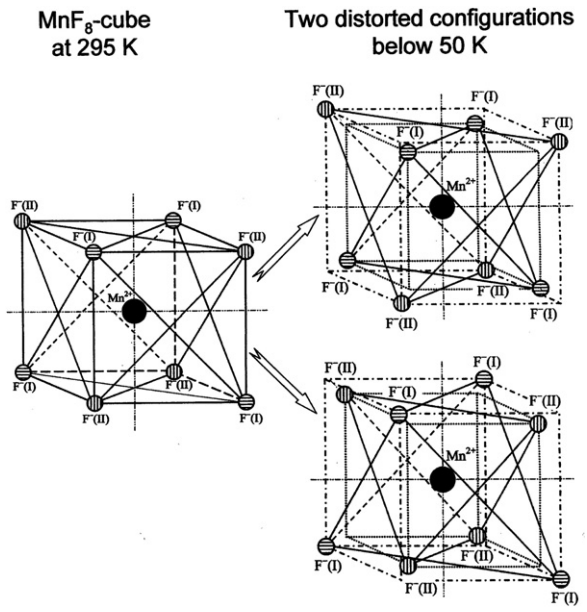

Figure 4. Cubic structure of MnF_8 at 295 K and its two equivalent deformations (to the two tetrahedra) below 50 K. The magnetic field direction for measurements along the [110] direction is marked.

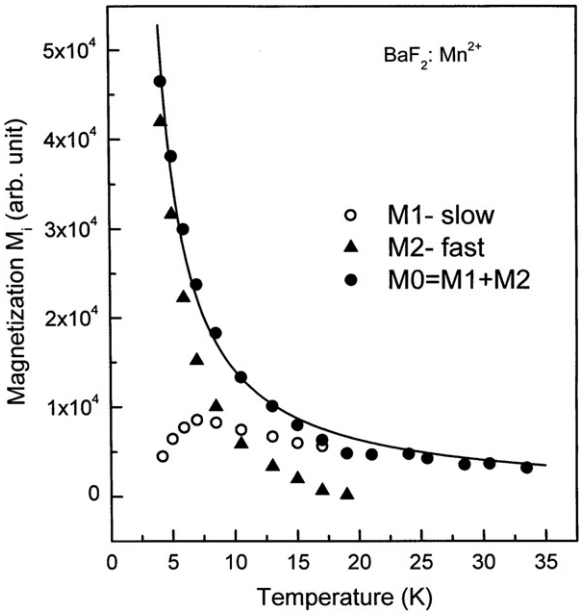

Figure 5. Temperature dependence of the slow (M_1) and fast (M_2) components of the total magnetization. The total magnetization M_0 of the spin system displays the Curie law behaviour (solid line).

3.2. Electron spin–lattice relaxation

The spin–lattice relaxation time T_1 characterizing recovery of the spin level population to the Boltzmann population was determined from the electron spin echo (ESE) amplitude. The ESE amplitude is proportional to the magnetization M_z after pulse excitation. The M_z recovery to the equilibrium value M_0 was double exponential for the cubic centre A at temperatures lower than 15 K and described as a sum of stretched exponential and pure exponential recovery:

$$M_z(t) = M_1\left[1-\left(1-\frac{D}{M_0}\right)\exp\left(-\frac{t}{\tau_{1\mathrm{slow}}}\right)^{\beta}\right] + M_2\left[1-\left(1-\frac{D}{M_0}\right)\exp\left(-\frac{t}{T_{1\mathrm{fast}}}\right)\right] \quad (2)$$

where M_0 is equilibrium magnetization value reached at the limit $t \to \infty$, D is the initial M_z-value after pulse saturation and $M_0 = M_1 + M_2$. β is a stretched coefficient. The two submagnetizations M_1 and M_2 vary in temperature as shown in figure 5. The temperature dependence of the total magnetization $M_0 = M_1 + M_2$ can be approximated by a Curie law as shown by the solid line in figure 5. It should be noted that the fast relaxation component dominates at the lowest temperatures and vanishes above about 15 K, whereas the slow stretched exponential component appears at the lowest temperatures and gradually grows, and $M_0 = M_{1\mathrm{slow}}$ above 15 K.

The stretched exponential recovery characterized by the relaxation time τ_1 (Kohlrausch law) is associated with a distribution of the relaxation time. The average relaxation time can be calculated as [25, 26]

$$\langle\tau_{1\mathrm{slow}}\rangle = T_{1\mathrm{slow}} = \int_0^{\infty}\exp\left[-\left(\frac{t}{\tau_{1\mathrm{slow}}}\right)^{\beta}\right]\mathrm{d}t = \frac{\tau_{1\mathrm{slow}}\Gamma\left(\frac{1}{\beta}\right)}{\beta} \quad (3)$$

where Γ denotes the gamma function, and $0 < \beta \leqslant 1$. The distribution of the relaxation time appears generally in amorphous and disordered solids, where it can be affected by temperature [27, 28]. For cubic Mn^{2+} centre A in BaF_2 the distribution is temperature independent with $\beta = 0.50 \pm 0.02$, which gives $\Gamma = 1$ and $T_{1\mathrm{slow}} = 2\tau_{1\mathrm{slow}}$. The two relaxation rates $1/T_{1\mathrm{slow}}$ and $1/T_{1\mathrm{fast}}$ grow with temperature as shown by full points in figure 6.

For the tetragonal centre B the magnetization recovery is single exponential in the whole temperature range, with a slow relaxation rate presented by open circles in figure 6.

The fast relaxation component of centre A was measured 40 years ago by the progressive saturation method [29]; however, the long component was then missed. The temperature dependence of $1/T_{1\mathrm{fast}}$ is typical for the Raman relaxation process as discussed in [29]. The dependence is described by the equation $1/T_1 = aT + bT^5$ with parameters $a = 25\,500\ \mathrm{s^{-1}\,K^{-1}}$ and $b = 14.5\ \mathrm{s^{-1}\,K^{-5}}$ (solid line in figure 6) for our results, and $a = 118\ \mathrm{s^{-1}\,K^{-1}}$, $b = 0.8\ \mathrm{s^{-1}\,K^{-5}}$ (dashed line in figure 6) from Horak's data [29]. The difference is due to the difference in Mn concentration in the studied crystals.

Ordinary relaxation processes cannot produce the slow, weakly temperature dependent relaxation that dominates above 15 K. Its temperature variation tends to the dependence $1/T_{1\mathrm{slow}} \propto T^2$ at high temperatures and is well described by

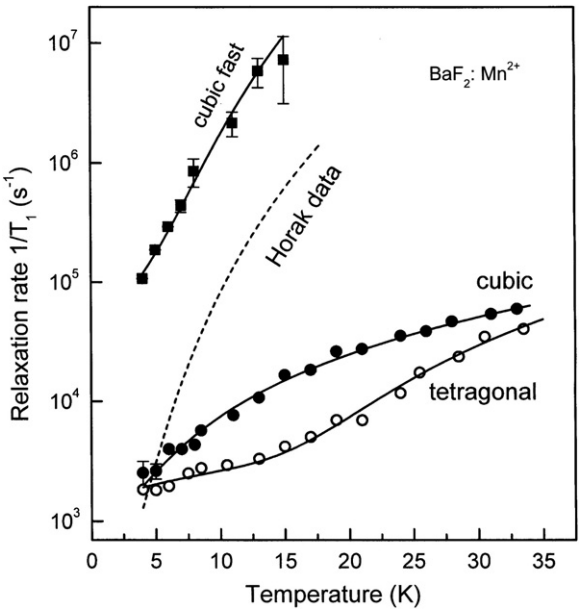

Figure 6. Temperature dependence of the spin–lattice relaxation rate $1/T_1$ for the fast and slow components of the double exponential recovery of the cubic centre A (full points) and for tetragonal centre B (open points). The solid lines represent a theoretical fit as described in the text. The dashed line shows the result of relaxation measurements of [28].

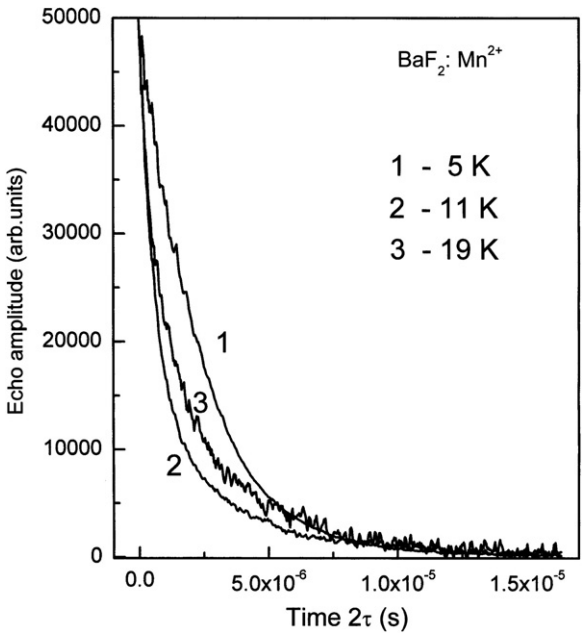

Figure 7. The electron spin echo decay curves at low temperatures showing the faster dephasing at 11 K compared to the lower (5 K) and higher (19 K) temperature.

the equation

$$\frac{1}{T_{1\text{slow}}} = c + aT + b\ \text{cosech}^2\left(\frac{E_{\text{vib}}}{2kT}\right) \tag{4}$$

where c is the temperature independent background from the cross-relaxation. The linear term aT generally appears in samples where the distribution of paramagnetic ions is not perfectly uniform [30]. The last term is characteristic for relaxation *via* a local vibration mode of energy E_{vib} [31]. The solid lines in figure 6 for the cubic and tetragonal centres are the best fits to equation (3) with parameters

$c = 0$, $a = 474\ \text{s}^{-1}\ \text{K}^{-1}$, $b = 6160\ \text{s}^{-1}$ and $E_{\text{vib}} = 17\ \text{cm}^{-1}$ for cubic centre A, and $c = 1448\ \text{s}^{-1}$, $a = 118\ \text{s}^{-1}\ \text{K}^{-1}$, $b = 2.5 \times 10^5\ \text{s}^{-1}$ and $E_{\text{vib}} = 78\ \text{cm}^{-1}$ for tetragonal centre B.

The above results show that the spin–lattice relaxation of Mn^{2+} impurities in BaF_2 is produced by the local dynamics but not by the lattice phonon. Only the cubic centre A relaxes effectively by phonons at low temperatures. However, the coupling of Mn^{2+} to phonons gradually vanishes on heating and becomes overdominated by the local vibration above 15 K. Such a behaviour is rather typical for amorphous materials [32, 33] where acoustic phonons have very short lifetime and are effectively scattered by soft local oscillators (local modes). When temperature increases the local modes are effectively excited, leading to a shortening of the phonon free path. When the phonon free path becomes comparable with the phonon wavelength the phonon concept as a plane wave loses meaning (Ioffe–Regel limit). A local distortion and a local vibration mode existing around Mn^{2+} impurities in BaF_2 are responsible for the weak coupling of the relaxing ions to the host lattice vibrations. The local distortion differs slightly from site to site, which is observed as a distribution of the relaxation time. The value of local mode energy $E_{\text{vib}} = 17\ \text{cm}^{-1}$ suggests that the mode can be a tunnelling motion between shallow potential wells and it was theoretically evaluated as $50\ \text{cm}^{-1}$ [24].

Tetragonal centre B, which exists in a relatively small concentration, relaxes also via a local mode but without a distribution of the relaxation time. The energy of this mode ($78\ \text{cm}^{-1}$) is typical for vibrational motions due to a phonon-assisted tunnelling between local deformations of the impurity complex in the host site as observed for Cu^{2+} in BaF_2 [19].

3.3. Electron spin echo dephasing (phase relaxation)

After pulsed excitation the perpendicular component of the magnetization, formed by a coherent precession of spins, decays in a time shorter than the spin–lattice relaxation time. This is due to a randomization of the precession phase of the excited spins. As a result, the amplitude of the ESE signal produced by the first pulse decays in time (typically in microseconds). The two-pulse ESE amplitude V decay is characterized by the so-called phase memory time T_{M}, which in the simple case of exponential decay is defined by the equation $V(\tau) = V_0 \exp(-2\tau/T_{\text{M}})$, where τ is the interpulse interval. The decay of ESE amplitude depends on temperature and it is shown in figure 7 for centre A. The ESE amplitude decay was described by the equation

$$V(t) = V_0 \exp\left(-at - mt^2\right) \tag{5}$$

at the lowest temperatures and above 20 K. The first term is due to temperature independent instantaneous diffusion produced by the second pulse as well as by molecular motions [34].

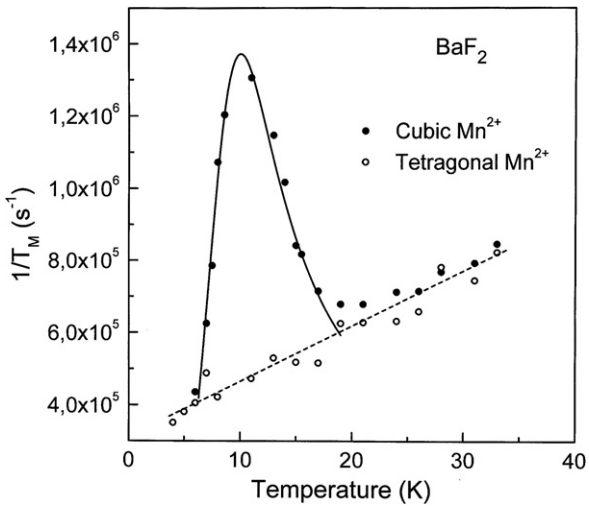

Figure 8. Temperature dependence of the dephasing rate $1/T_M$ for cubic (full circles) and tetragonal (open circles) Mn^{2+} centres in BaF_2. The solid line around the maximum is the best fit with equation (8). The straight line describes continuous temperature broadening of the spin packets forming the individual hyperfine EPR line of the tetragonal centre.

This term dominates in the whole temperature range. The second term arises from the spectral diffusion and gives a small contribution at the lowest temperatures only. From the fit of equation (5) to experimental decay at various temperatures the phase memory time was calculated as described in paper [34]. In the intermediate temperature range the decay was clearly non-exponential and time T_M was determined as the time where the ESE amplitude decreases to $1/e$ of the initial value. The ESE decay curves around 11 K are shown in figure 7.

The dephasing rate $1/T_M$ depends on temperature as shown in figure 8 both for dominant cubic centre A and the weak tetragonal centre B. The background temperature dependence is identical for the two centres and is due to molecular motions producing continuous broadening of the spin packets on heating. A contribution from the spin–lattice relaxation process is negligible. Around 10 K the dephasing rate displays strong resonance-type acceleration due to a specific molecular motion.

Any motional process producing a collapse of the spin packets will give a resonance enhancement of the dephasing rate when the frequency of the motion changes from the slow to the fast motion range as compared to the packet splitting 2Δ. The spin packets form an inhomogeneously broadened EPR line and are doublets at $B_0 \pm \Delta$ due to electron–^{19}F nucleus dipolar coupling. These nuclei belong to the distant fluorine ions (>0.5 nm), which do not produce resolved splitting in the EPR spectrum. Various processes producing dephasing have been considered: spin–lattice relaxation processes [35], methyl group reorientations [36, 37], random modulations of the longitudinal spin component [38], and spectral diffusion in a spin system [39]. According to [35] the expression for the decay of the two-pulse ESE amplitude $V(2\tau)$ due to the dynamical process characterized by the correlation time τ_c has the form

$$V(2\tau) = \frac{V_0}{R^2}\exp\left(-\frac{2\tau}{\tau_c}\right)\left[\frac{1}{\tau_c^2}\sinh^2(R\tau) + R^2\cosh^2(R\tau) + \Delta^2\sinh^2(R\tau) + \frac{R}{\tau_c}\sinh(2R\tau)\right] \quad (6)$$

where $R^2 = \tau_c^{-2} - \Delta^2$ and τ is the interpulse interval. This equation shows that the ESE amplitude decay in the range of collapsing spin packets is complex and non-exponential and the phase memory time T_M cannot be directly defined. Assuming that the dynamical process is thermally activated, with correlation time dependent on temperature as given by the Arrhenius equation $\tau_c = \tau_0\exp(E_a/kT)$, one can calculate the temperature dependence of the effective T_M, which shows a resonance-type maximum in the dephasing rate. Usually at low temperatures, below 50 K, the Δ^2 value becomes larger than τ_c^2 and only the high temperature region can be calculated from equation (6). Simplified forms of the decay function in the fast and slow motion regions can be easily derived. For slow motion with $\tau_c^{-1} \ll \Delta$, the decay is described by $V(2\tau) \simeq V_0\exp(-2\tau/\tau_c)$ with $T_M = \tau_c$. For fast motion ($\tau_c^{-1} \gg \Delta$), the decay function is $V(2\tau) \simeq V_0\exp(-\Delta^2\tau_c\tau)$ with $T_M = 2/(\Delta^2\tau_c)$. From these simple expressions and the Arrhenius equation we evaluated the activation energy of the dynamical process as $E_a = 25\ \text{K} = 17\ \text{cm}^{-1}$ and $\tau_0 = 4\times10^{-8}$ s in the slow motion limit, and $\Delta^2\tau_0 = 3.4\times10^5\ \text{s}^{-1}$ in the fast motion limit, which gives $\Delta = 3\ \text{MHz} = 0.11$ mT.

Another approach is based on considerations of the fluctuating local magnetic field B_{loc} produced by the nuclei. This approach is generally used in NMR spectroscopy for description of the resonance enhancement of the spin–lattice relaxation. For the exponential correlation function of the fluctuations the relaxation rate is [40]

$$\frac{1}{T_1} = \frac{2}{\hbar^2}\left|\left\langle -\frac{1}{2}\right| H \left|\frac{1}{2}\right\rangle\right|^2 B_{loc}^2\frac{\tau_c}{1+\omega_0^2\tau_c^2} \quad (7)$$

where H is the dipolar perturbation Hamiltonian and ω_0 is the resonance frequency.

When fluctuations are produced by spin jumps between two orientations having resonance lines split by $\Delta\omega$, then [40, 41]

$$\frac{1}{T_1} = \frac{1}{6}\Delta\omega^2\frac{\tau_c}{1+\omega_0^2\tau_c^2}. \quad (8)$$

Equation (8) describes well the shape of the temperature dependence around the maximum as shown by solid line in figure 8 for the cubic Mn^{2+} centre. However, only the activation energy $E_a = 31\ \text{K} = 21\ \text{cm}^{-1}$ is an acceptable fit parameter. Thus, this approach gives a qualitative description only.

The individual line width is 0.46 mT at 5 K and the spin packet width can be evaluated from time T_M as $\Delta B_{packet} = 2\hbar(\sqrt{3}g\,\mu_B T_M)^{-1} = 2.6\ \mu$T at 5 K. The splitting of the unresolved lines of spin packets which undergo dynamical averaging is $2\Delta = 0.22$ mT, thus the packets are formed by not very distant fluorine nuclei, which may be located in the second coordination sphere. This Mn–F distance cannot be evaluated from the point dipole approximation because of the

dominant contribution from isotropic hyperfine coupling [8]. The dynamics which averages the dipolar Mn–F splitting is characteristic for the cubic Mn^{2+} centre only. The tetragonal centre does not display resonance dephasing acceleration in the studied temperature range, as is visible in figure 8. This specific motion has to be related to the low temperature deformation of the MnF_8 cube into the two tetrahedra. This transition leads to the two possible sites for the coordinated fluorine ions. The deformations are not static, as was assumed previously, since the jumps between these two positions are visible in the spin relaxation. The jumps are due to the tunnelling motion at frequency 4×10^8 s^{-1} through the low energy barrier $E_a = 17$ cm^{-1}. This is also observed as the local mode of energy $E_{vib} = 17$ cm^{-1} of the manganese complex, which we also identified during the spin–lattice relaxation measurements as described above. The jumps of fluorine ions produce a decoherence of the ^{19}F precession motion, precluding the appearance of the modulations of the electron spin echo decay.

4. Conclusions

We confirm that a structural transition appears at about 45 K around Mn^{2+} in BaF_2 lattice. As a result, the MnF_8 cube is deformed into two tetrahedra of different dimensions with Mn^{2+} in T_d symmetry. We confirmed this specific type of deformation by computer simulation of the change in the ^{19}F hyperfine structure of the EPR spectra. The spin relaxation data at low temperatures show that after the deformation there exists a local dynamics described as jumps between the two tetrahedral deformations via a low energy barrier $E_a = 17$ cm^{-1} with tunnelling frequency 4×10^8 s^{-1}. This dynamics is directly visible as the dominant electron spin echo (ESE) dephasing mechanism around 11 K. This motion is also visible as a local mode vibration governing the temperature dependence of the spin–lattice relaxation. The local mode overdominates the coupling to the lattice phonons above 11 K.

The obtained results indicate that pulsed EPR measurements of the electron spin relaxation are a powerful method in studies of local molecular dynamics.

References

[1] Kanchana V, Vaitheeswaran G and Rajagopalan M 2003 *J. Alloys Compounds* **359** 66

[2] Hayes W (ed) 1974 *Crystals with the Fluorite Structure: Electronic, Vibrational and Defect Properties* (Oxford: Clarendon)

[3] Gehlhoff W and Ulrici W 1980 *Phys. Status Solidi* b **102** 11

[4] de Lucas M C M, Moreno M, Rodriguez F and Baranov P G 1996 *J. Phys.: Condens. Matter* **8** 2457

[5] Danilkin M, Lust A, Kerikmae M, Seeman V, Mandar H and Must M 2006 *Radiat. Meas.* **41** 677

[6] Soethe H, Vetrov V A and Spaeth J-M 1992 *J. Phys.: Condens. Matter* **4** 7927

[7] Alcala R, Pena J I and Alonso P J 1989 *J. Phys.: Condens. Matter* **1** 8217

[8] Barriuso M T, Baranov P G and Moreno M 1991 *Radiat. Eff. Defects Solids* **119–121** 177

[9] Badalyan A G, Baranov P G, Vikhnin V S and Khramtsov V A 1986 *Pis. Zh. Eksp. Teor. Fiz.* **44** 87 (Russia)

[10] Alcala R, Alonso P J and Cases R 1983 *J. Phys. C: Solid State Phys.* **16** 4693

[11] Alonso P J and Alcala R 1985 *Phys. Status Solidi* b **128** K153

[12] Nakata R, Kohno K, Sumita M and Higuchi E 1976 *J. Phys. Soc. Japan* **41** 470

[13] Orera V M, Alonso P J, Cases R and Alcala R 1984 *Radiat. Eff.* **83** 213

[14] Alonso P J and Alcala R 1985 *Phys. Status Solidi* b **127** K77

[15] Smoluchowski R 1969 *Magnetic Resonance and Radiofrequency Spectroscopy—Proc. 15th Coll. AMPERE* (Amsterdam: North-Holland) p 120

[16] Hoffmann S K and Ulanov V A 2000 *J. Phys.: Condens. Matter* **12** 1855

[17] Sochava L S, Tolparov Y N and Kovalev N N 1971 *Fiz. Tverd. Tela* **13** 1463
Sochava L S, Tolparov Y N and Kovalev N N 1971 *Sov. Solid State Phys.* **13** 1219 (Engl. Transl.)

[18] Vikhnin V S, Sochava L S and Tolparov Y N 1979 *Fiz. Tverd. Tela* **21** 1789
Vikhnin V S, Sochava L S and Tolparov Y N 1979 *Sov. Solid State Phys.* **21** 1023 (Engl. Transl.)

[19] Hoffmann S K, Goslar J, Lijewski S and Ulanov V A 2007 *J. Chem. Phys.* **127** 124705

[20] Richardson R J, Lee S and Menne T J 1971 *Phys. Rev.* B **4** 3837

[21] Zhang Y P, Buckmaster H A and Kudynska J 1995 *Fuel* **74** 1307

[22] Wieckowski A and Kulinski W 1975 *Acta Phys. Pol.* A **47** 481

[23] Radhakrishna S, Chowdari B W R and Viswanath A K 1976 *J. Phys. Soc. Japan* **41** 1530

[24] Garcia-Fernandez P, Aramburu J A, Barriuso M T and Moreno M 2008 *J. Chem. Phys.* **128** 124513

[25] Lai P Y 1995 *Chin. J. Phys.* **33** 271

[26] Hall D B, Dhinojwala A and Torkelson J M 1997 *Phys. Rev. Lett.* **79** 103

[27] Huber D L 2000 *J. Lumin.* **86** 95

[28] Hoffmann S K, Hilczer W, Goslar J, Kiczka S and Polus I 2002 *Phys. Chem. Chem. Phys.* **4** 4944

[29] Horak J B and Nolle A W 1967 *Phys. Rev.* **153** 372

[30] Hoffmann S K, Hilczer W, Goslar J and Augustyniak-Jablokow M 2001 *J. Phys.: Condens. Matter* **13** 7443

[31] Maradudin A A 1966 *Solid State Physics* vol 19 (New York: Academic)

[32] Klinger M I 1998 *Phys. Rep.* **165** 275

[33] Courtens E, Foret M, Hehlen B and Vacker R 2001 *Solid State Commun.* **117** 187

[34] Hoffmann S K, Goslar J, Hilczer W, Augustyniak-Jablokow M A and Kiczka S 2001 *J. Magn. Reson.* **153** 56

[35] Zhidomirov G M and Salikhov K M 1969 *J. Exp. Theor. Phys.* **56** 1933 (Russia)

[36] Tsvetkov Yu D and Dzuba S A 1990 *Appl. Magn. Reson.* **1** 179

[37] Zecevic A, Eaton G R, Eaton S S and Lindgren M 1998 *Mol. Phys.* **95** 1255

[38] Milov A D, Salikhov K M and Tsvetkov Yu D 1972 *J. Exp. Theor. Phys.* **63** 2329

[39] Kurshev V V and Ichikawa T 1992 *J. Magn. Reson.* **96** 563

[40] Slichter C R 1990 *Principles of Magnetic Resonance* (Berlin: Springer) chapter 5.10

[41] Eaton S S and Eaton G R 2000 *Biological Magnetic Resonance* vol 19 *Distance Measurements in Biological Systems by EPR* ed L J Berliner, S S Eaton and G R Eaton (New York: Kluwer) chapter 2